Unimolecular Decomposition of Formaldehyde: $H_2CO \rightarrow H_2 + CO$. Part I: Ab Initio Reaction Path and Variational Transition State Rate Constants

Leila M. M. de A. Martins, Graciela Arbilla,* and Edilson C. da Silva

Instituto de Química, Departamento de Fisico-Química, Universidade Federal do Rio de Janeiro, Cidade Universitária, Rio de Janeiro, RJ, 21949-900, Brazil

Received: July 10, 1998; In Final Form: October 1, 1998

Features of the ground-state potential energy surface of formaldehyde relevant to its dissociation to H_2 and CO were analyzed by means of ab initio calculations. The multiconfigurational self-consistent field (MCSCF) calculation gave a critical energy of 83.22 kcal/mol. Accurate structures are presented for $H_2CO(X^1A_1)$ and the saddle point. The reaction path was determined and the coupling between reaction coordinate and normal modes was analyzed along it, with two different levels of calculation (Hartree−Fock and MCSCF). Using these data, the transition state was located and the rate constants were calculated for the temperature range 200−4500 K using the generalized transition state theory.

Introduction

The formaldehyde molecule has been the focus of many experimental and theoretical studies since the seventies[1,2] due to its importance in the atmosphere, interestellar space, and combustion chemistry. Also its small size allows ab initio calculations at a high level of theory as well as trajectory and variational transition state studies. Presently, the mechanism of photodissociation is well-known due largely to the work of Moore and co-workers.[1−6] The electronically excited $H_2CO(S_1)$ internally converts to highly vibrationally excited levels of the ground electronic state (S_0) which then undergoes unimolecular reaction by two different pathways: one producing molecular products ($H_2 + CO$) and the other producing radical products (HCO + H). This last channel has been recently studied by Terentis and Kable.[7]

As previously discussed,[7−8] ab initio theoretical calculations show that the S_0 state correlates with both molecular and ground-state radical products while the S_1 state correlates with excited-state HCO. Several calculations have been conducted for both the radical and molecular dissociation of S_0, S_1, and T_1 formaldehyde,[8−13] in particular the activation energy for dissociation to $H_2 + CO$ on the ground S_0 potential energy surface. Some theoretical studies[8,9] gave an estimated activation energy of 87 kcal/mol. This means that quantum mechanical tunneling must probably be invoked in order to account for dissociation products observed at energies near the S_1 origin at 3.495 eV (80.6 kcal/mol). More recent calculations[10,11] gave values near the origin, which implies that low-energy dissociation may occur without tunneling.

Theoretical studies of this reaction have been basically concerned with the determination of the properties of stationary points (i.e., the equilibrium state and the saddle point) and also on investigating the possibility of an intermediate state.[8−14] Classical trajectory calculations have been carried out by Chang, Minichino, and Miller[15] using a global potential energy surface constructed using the empirical valence-bond approach. Specific rate constants using RRKM theory with tunneling corrections were calculated by Miller[17] and later by Troe,[18] who also analyzed the rotational contributions to the rate constants. Despite the extensive work done on this reaction, to our knowledge the complete reaction path has not been calculated and the generalized transition state theory[19] has not been applied in order to get thermal rate constants.

In this work, the stationary points of the potential energy surface were determined at a high level of calculation and the reaction path connecting the stable and saddle points was calculated using the "intrinsic reaction coordinate" (IRC) approach.[19] Then, using the direct dynamics approach, the ab initio electronic structure information for the region of configuration space along the reaction path was used to calculate the variational transition state theory (VTST) rate constants, including tunneling effects.[19−21]

Unfortunately, these calculations are not suitable for comparison with photochemical experimental data and previous microcanonical calculations since they were obtained for a different energy distribution. Nevertheless, since the electronic structure data may be obtained at a high level of theory, this system is a good test for the electronic input methodology in the calculation of thermal rate constants. Furthermore, the complete reaction path calculated at a high level of theory and the conclusions obtained by the variational optimization of the location of the generalized transition state theory dividing surface are extremely important information for the variational calculation of the microcanonical rate constants.[22] Also, since this reaction path presents a well-defined barrier, in contrast to the HCO + H channel on the S_0 surface, which presents a barrierless pathway, a further test of the direct dynamics approach may be done.[22]

Methods and Computational Details

The MCSCF Wave Function. Although the Hartree−Fock (HF) wave function alone provides a good approximation to the absolute energy of a molecule, it does not work for correlation effects. Thus, for an adequate description of bond breaking and bond formation, as well as the barrier height involved in these processes, it is necessary to use high-quality wave functions beyond the HF approximation. Let us consider

* Author to whom correspondence should be addressed.

10.1021/jp982962m CCC: $15.00
Published on Web 12/03/1998

the planar C_{2v} structure of the ground state and dissociation products of formaldehyde:[12]

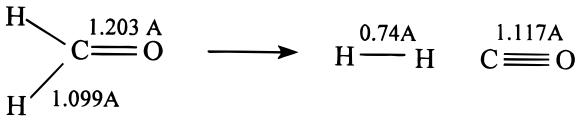

Now we consider the correlation between the electronic states of the reactant and the products. As can be seen, four electrons, the ones involved in the two C−H bonds of H_2CO, are active in the dissociation process. During the dissociation process, two electrons, one for each C−H bond, pair up to form the H−H bond, while the other two form a lone pair on C in CO.

The formaldehyde molecule has a doubly occupied σ (in-plane) lone pair orbital on O. During dissociation to H_2 + CO, this orbital delocalizes toward C and finally becomes the third component of the triple bond in ground state CO. Correlation effects associated with this orbital should change significantly during dissociation.

During dissociation, the CO bond shortens as it acquires more triple-bond character. A proper description of this bond shortening requires proper consideration of the ($\sigma-\pi$) correlation effects.

Therefore, an accurate description of the potential energy surface near this barrier requires a balanced treatment of both diabatic states, which cannot be achieved within the HF model. However, MCSCF calculations based on a HF reference can yield results of high accuracy, provided the right choice of the active space has been made, leading to the correct behavior of the molecule under dissociation. Further (dynamic) correlation can be recovered in more extensive CI calculations.

Basis Sets and Geometry Optimization. The basis set used in our calculations consists of the Huzinaga−Dunning double-ζ [(9s5p/4s)/(6s3p/3s)][23] basis, augmented with a set of d polarization functions on each carbon and oxygen atom, with exponents $\alpha_O = 0.8$ and $\alpha_C = 0.75$, and a set of p functions on hydrogen with $\alpha_p = 1.0$. This DZP basis set comprises forty-two functions.

The geometries of the reactant, the products, and the transition state were optimized at the restricted Hartree−Fock (RHF), generalized valence bond (GVB), and multiconfigurational self-consistent field (MCSCF) levels, using the gradient capability of the GAMESS package.[24] In the GVB calculations we have included all but the lone-pair valence electron on the oxygen atom (GVB4PP). In the MCSCF calculations, we have considered four, six, and 10 active electrons; these calculations will be denoted by MCSCF4, MCSCF6, and MCSCF10, respectively.

Ab Initio Reaction Path and Direct Dynamics Calculations. The thermal rate constants were calculated on the basis of an ab initio reaction path (Figure 1), its curvature, and an harmonic approximation to the potential orthogonal to it, without the intermediate step of fitting the potential energy surface. The geometries of the stationary points were optimized both at Hartree−Fock (HF) and multiconfiguration self-consistent field (MCSCF) levels. The calculated saddle-point geometries were used as starting points to evaluate the IRC by going downhill to both the asymptotic reactant and products channels in mass-weighted coordinates. The details of the approach used to obtain a minimum energy path (MEP), well-enough converged to calculate accurate thermal rate constants within the framework of the generalized transition state, are fully described by Truhlar and co-workers[20] and are briefly presented below.

The canonical rate constants, $k(T)$, were calculated using the generalized transition state theory (GTST) as implemented in

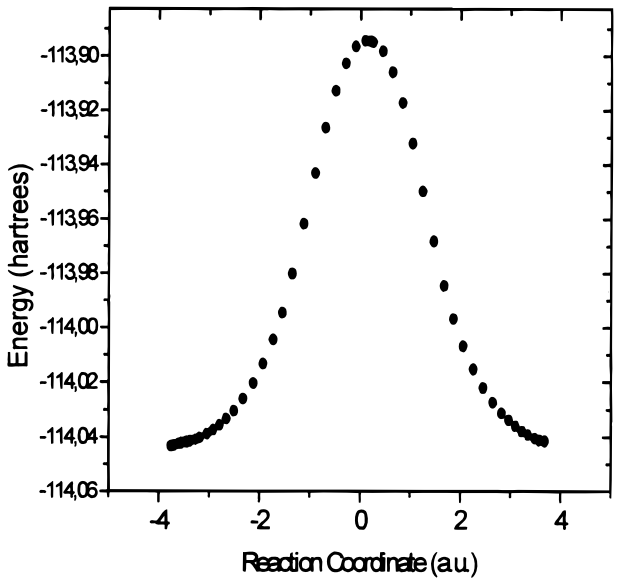

Figure 1. Calculated energy along the reaction path for the reaction $H_2CO \rightarrow H_2 + CO$. The curve was obtained at MCSCF level using a $0.001a_0$ step size.

the POLYRATE program,[25] which assumes that the net rate of forward reaction at equilibrium is given by the flux of trajectories across a critical dividing surface in the phase space in the product direction. Within the variational approach, the position of this dividing surface, designated by s_T, may be treated as a variable to be determined by the variational principle of minimizing the calculated $k(T)$, which is referred to the maximum free energy criterion. The location of the canonical variational transition state is temperature-dependent and the calculated rate constant gives the best canonical average at each temperature.[26] Some details of the calculation are given below.

Method of Locating the Saddle Point. To locate the saddle point, an initial guess of the position of the transition state must be provided.[27] For this purpose, an approximated three-dimensional surface for the ground-state dissociation pathway ($H_2CO \rightarrow H_2 + CO$) was calculated, assuming a C_{2v} geometry. By changing the r(CH) distance and the θ(HCH) angle, the gray scale map shown in Figure 2 was obtained at Hartree−Fock level.

The geometry (C_{2v}) obtained for the initial guess was r(CH) = 1.3904 Å and θ(HCH) = 158.9°, with the other distances and angles equal to those of the formaldehyde molecule (Table 1). Starting from this geometry, the energy gradients were evaluated using the algorithm of Cerjean and Miller.[28] This method uses the second derivative matrix (i.e., the force constants) of the potential surface to walk uphill to the saddle point.

After obtaining the right number of negative eigenvalues for the Hessian at this level of calculation, we determined the saddle point at the other levels using the Hartree−Fock saddle point as an initial guess. The saddle point has C_s symmetry at all the calculated levels.

The Minimum Energy Path. The path beginning in the direction of negative curvature away from the transition state and following the gradient of the potential energy surface to the reactant and products is called the reaction path or the intrinsic reaction coordinate (IRC).

Starting from the saddle point geometry and going downhill to both the asymptotic reactant and product channels, the intrinsic reaction coordinate was constructed. Several step sizes, between $0.2a_0$ and $0.001a_0$ were tested in order to ensure

TABLE 1: Ab Initio Geometric Parameters of Reactant and Saddle Point

	parameters[a]	experimental values	calculated values				
			HF	MC4	MC6	GVB4	MC10
H_2CO	r (CO)	1.203 ± 0.003	1.189	1.188	1.186	1.188	1.224
	r (CH)	1.099 ± 0.009	1.096	1.118	1.120	1.118	1.122
	θ (OCH)	121.75 ± 0.6	121.85	122.12	122.24	122.12	122.14
saddle point	r (CO)		1.147	1.160	1.158	1.184	1.188
	r (CH1)		1.099	1.098	1.098	1.082	1.096
	r (H1H2)		1.224	1.350	1.371	1.337	1.383
	θ (H1CO)		162.60	162.25	163.80	162.05	164.19
	θ (CH1H2)		87.53	86.97	87.27	85.25	87.65

[a] In angstroms and degrees.

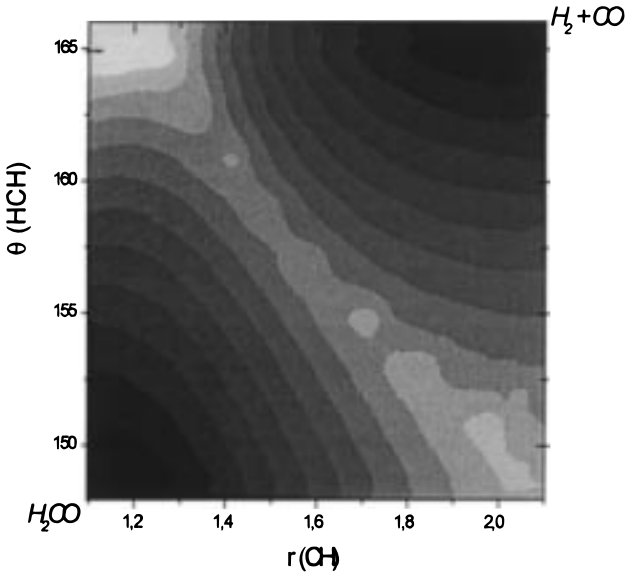

Figure 2. Approximated potential energy surface for the decomposition of a formaldehyde molecule as a function of the C−H distance and the HCH angle.

convergence. Along this minimum energy path (MEP), the reaction coordinate is defined as the signed distance from the saddle point, with $s > 0$ referring to the product side. In this work the reduced mass was set equal to 1 μ ($\mu = 1$ ^{12}C atomic mass unit) and, then, the distances along the mass-scaled coordinates in a_0 are equivalent to distances through mass-weighted coordinates in units of bohr amu$^{1/2}$. These calculations were performed both at HF and MCSCF levels using the GAMESS program.

The matrix of force constants, at the HF and MCSCF levels, were then computed for seven selected points on each side of the reaction path and the three stationary points (reactant, saddle point, and products). Finally, a generalized normal-mode analysis was performed by projecting out the frequencies at each point.[29] The variational partition function along the MEP and the vibrationally adiabatic ground-state potential curve were then calculated using the POLYRATE program. This potential is defined as:

$$V_a^G(s) = V_{MEP}(s) + \epsilon_{int}^G(s)$$

where $V_{MEP}(s)$ is the classical energy along the MEP with its zero energy at the bottom of the vibrational well for the reactant and $\epsilon_{int}^G(s)$ is the total vibrational zero-point energy at s.

Rate Constants Calculations. Within the framework of the generalized transition state theory (GTST), for a canonical ensemble of a reacting classical system, characterized by a temperature T, the conventional transition state rate constant is the equilibrium one-way flux coefficient of phase−space trajetories through the dividing surface at $s = 0$ in the product direction. The classical generalized transition rate constant, $k_c^{GT}(T,s)$ at temperature T, is defined as

$$k_c^{GT}(T,s) = \frac{\sigma\, Q_c{}^{GT}(T,s)}{\beta h\, \Phi_c{}^R(T)} \exp(-\beta V_{MEP}(s))$$

where β is, as usual, $(k_B T)^{-1}$, k_B is Boltzmann's constant, h is the Planck constant, $Q_c{}^{GT}(T,s)$ is the classical partition function for the generalized transition state (GTS) dividing surface with its zero of energy at $V_{MEP}(s)$ and with all rotational symmetry numbers set to unity, $V_{MEP}(s)$ is the classical potential energy at point s on the MEP relative to the overall zero of energy, Φ_c^R is the reactant classical partition function per unit volume, and σ is the symmetry factor.

For a fixed temperature the lowest upper bound on the true classical rate constant for the assumed set of GTS dividing surfaces is found by varing the location of the GTS in order to minimize $k_c^{GT}(T,s)$. Thus the classical CVT(Canonical Variational Theory) rate constant $[k_c{}^{CVT}(T)]$ is given by

$$k_c^{CVT}(T) = \min_s k_c^{GT}(T,s)$$
$$= k_c^{GT}(T,s_c^{CVT}(T))$$

where $s_c^{CVT}(T)$ is the location of the CVT transition state for temperature T.

In this work quantal effects on the partition functions for the bound degrees of freedom were incorporated and, thus, a "hybrid" generalized canonical TST rate constant $k^{CVT}(T)$ was calculated. The dividing surface for this constant is denoted by $s^{CVT}(T)$.

When calculating $k^{CVT}(T)$ the motion along the reaction coordinate is treated classically. This result may underestimate the true quantal rate constant, mainly at low temperatures. The usual way of including the quantum effects on reaction−coordinate motion is by using a multiplicative transmission coefficient $\kappa(T)$:

$$k^{CVT/W}(T) = \kappa^{CVT/Y}(T) k^{CVT}(T)$$

The simplest way of evaluating $\kappa^{CVT/Y}$ is by using the semiclassical Wigner correction which gives reasonable results only at high temperatures, where the transmission coefficient is near unity and the potential along the reaction path is well approximated as an inverse parabola with a small reaction-path curvature.

A more accurate correction for systems with small reaction-path curvatures is obtained by assuming that the dominant quantal correction to reaction-coordinate motion comes from tunneling through the saddle point region. If the barrier is

TABLE 2: Energies of Formaldehyde and Saddle Point

	method	energy (h)	energy (h)[a]
formaldehyde	HF	−113.894	−113.894
	SDHF	−114.223	−114.195
	GVB4(C═O, C−H)	−113.962	
	MC4	−113.937	−113.929
	MC6	−113.940	−113.940
	MC10	−114.044	−114.045
saddle point	HF	−113.727	−113.726
	SDHF	−114.065	−114.039
	GVB4(C═O,C−H)	−113.818	
	MC4	−113.779	−113.779
	MC6	−113.793	−113.793
	MC10	−113.902	−113.902

[a] These values were taken from ref 10.

TABLE 3: Correlation Effects on the Barrier Height[a]

methods	ΔE (kcal/mol)	E_0 (kcal/mol)	E_0[b] (kcal/mol)
HF	105.3	99.7	99.4
SDHF	99.2		92.8
GVB4	90.7		
MC4	94.1	88.5	88.7
MC6	91.8	86.4	
MC10	89.0	83.2	84.4

[a] E_0 critical energy for decomposition reaction. [b] These values were taken from ref 10.

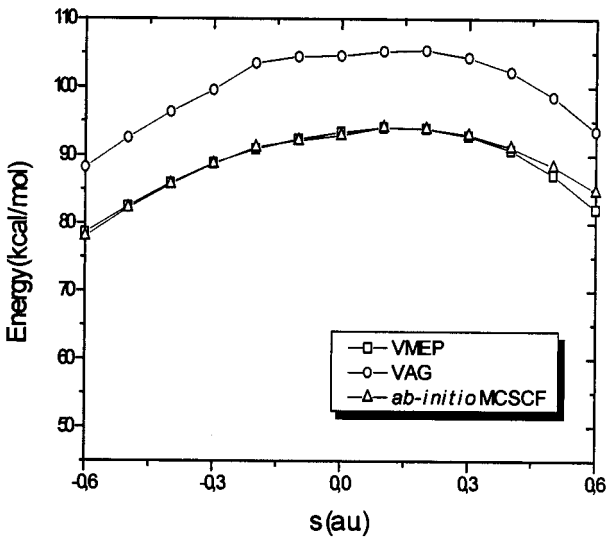

Figure 3. Classical potential energy curve(V_{MEP}), and vibrationally adiabatic potential energy curve V_a^G as a function of the distance along the MEP calculated using POLYRATE. The ab initio MEP is also shown.

assumed to be parabolic in the region of the maximum, the semiclassical transmission coefficient may be described by the zero-curvature (ZCT) or MEPSAG coefficient.[19] While in the canonical variational theory a single generalized transition state is optimized for a canonical ensemble, in the improved canonical variational theory (ICVT) the generalized transition state is optimized microcanonically for energies up to the microcanonical variational threshold energy (i.e., a separate generalized transition state is optimized for each total energy). For higher energy contributions, the generalized transition state is optimized canonically.

In this work the following levels of calculation of the canonical rate constants were considered: conventional transition state theory (TST), canonical variational transition state theory (CVT), and improved canonical variational theory (ICVT). For both TST and CVT rate constants, the classical

TABLE 4: Harmonic Vibrational Frequencies (cm^{-1}) of the Reactant and Saddle Point Calculated at HF and MCSFT Levels

formaldehyde			
normal mode	expt[a]	HF	MCSCF
$\nu_1(a_1)$ CH + CH stretch	2944	3183	3120
$\nu_2(a_1)$ CO stretch	1764	1925	1886
$\nu_3(a_1)$ CH_2 sym. bend	1563	1647	1537
$\nu_4(b_1)$ CH_2 out-of-plane	1191	1370	1255
$\nu_5(b_2)$ CH−CH stretch	3009	3103	3054
$\nu_6(b_2)$ CH_2 sym. bend	1287	1351	1141

saddle point		
normal mode	HF	MCSCF
$\nu_1(a')$	3252	3127
$\nu_2(a')$	2102	1817
$\nu_3(a')$	1473	1238
$\nu_4(b')$	800	845
$\nu_5(b')$	2269*i*	1735*i*
$\nu_6(b'')$	1029	796

TABLE 5: Bottleneck Properties of the $H_2CO \rightarrow H_2 + CO$ Reaction[a]

			V_{MEP} (kcal/mol)	
T (K)	s^b_{HF}	s^b_{MCSCF}	HF	MCSCF
	0.0	0.0		
200	0.0121	0.1650	105.32	94.07
250	0.0122	0.1650	105.32	94.07
298.5	0.0122	0.1651	105.32	94.07
300	0.0122	0.1651	105.32	94.07
350	0.0122	0.1652	105.32	94.07
400	0.0122	0.1653	105.32	94.07
450	0.0122	0.1655	105.32	94.07
600	0.0120	0.1665	105.32	94.07
800	0.0155	0.1683	105.32	94.06
1000	0.0109	0.1704	105.32	94.05
2000	0.0094	−0.1115	105.32	92.25
4500	0.0103	−0.1318	105.62	91.98

[a] Based on the CVT method. [b] Units of bohr $amu^{1/2}$.

transmission coefficients (CAG) for correcting the classical threshold were evaluated. Finally, quantum effects on the reaction coordinate motion were included by calculating the transmission coefficients considering small reaction-path curvature, i.e., assuming that the dominant quantal correction comes from tunneling through the saddle point region. Two approaches were used: semiclassical Wigner corrections[10] and tunneling along MEP with zero curvature (ZCT).[30−35]

Results and Discussion

Transition State and Activation Energy. The geometric parameters and calculated energies for formaldehyde and the saddle point are shown in Tables 1 and 2, respectively. In Tables 1, 2, and 3, the MCSCF wave functions including all configurations generated by distributing four, six, and 10 electrons in an equal number of orbitals are denoted MC4, MC6, and MC10, respectively.

The correlation effects on the barrier height are shown in Table 3. All the results were obtained with the DZP basis set. Table 4 shows the harmonic vibrational frequencies of the reactant and saddle point calculated at HF and MCSCF levels.

The calculated geometries for the formaldehyde molecule are in good agreement with the experimental values while the frequencies are slightly overestimated. Similar trends may be expected for the calculated saddle point properties. The calculated barrier heights are in excellent agreement with previously

TABLE 6: Forward Rate Constants (s^{-1}) Using Hartree−Fock Level to Scale the PES

T (K)	TST	TST/CAG	CVT	CVT/CAG	ICVT	TST/W	TST/ZCT	CVT/ZCT	ICVT/ZCT
200.00	9.5316E−97	9.3148E−97	9.3097E−97	9.3097E−97	9.4236E−97	1.1535E−95	2.5697E−43	2.5683E−43	2.5997E-43
250.00	7.4700E−75	7.3338E−75	7.3290E−75	7.3290E−75	7.3892E−75	6.0544E−74	1.4024E−39	1.4015E−39	1.4130E-39
298.50	1.3194E−60	1.2992E−60	1.2984E−60	1.2984E−60	1.3058E−60	7.8950E−60	4.0337E−37	4.0310E−37	4.0543E-37
300.00	3.0749E−60	3.0281E−60	3.0261E−60	3.0261E−60	3.0434E−60	1.8246E−59	4.6738E−37	4.6706E−37	4.6973E-37
350.00	8.7343E−50	8.6203E−50	8.6149E−50	8.6149E−50	8.6498E−50	4.0396E−49	3.2342E−35	3.2321E−35	3.2452E-35
400.00	6.2065E−42	6.1355E−42	6.1322E−42	6.1322E−42	6.1500E−42	2.3432E−41	8.7444E−34	8.7395E−34	8.7651E-34
450.00	8.1088E−36	8.0263E−36	8.0229E−36	8.0229E−36	8.0398E−36	2.5891E−35	2.1545E−32	2.1535E−32	2.1581E-32
600.00	1.5001E−23	1.4886E−23	1.4886E−23	1.4886E−23	1.4898E−23	3.3505E−23	8.8962E−23	8.8959E−23	8.9032E-23
800.00	2.6415E−14	2.6263E−14	2.6275E−14	2.6275E−14	2.6280E−14	4.4743E−14	5.9840E−14	5.9865E−14	5.9879E-14
1000.00	9.9264E−09	9.8808E−09	9.8879E−09	9.8879E−09	9.8885E−09	1.4334E−08	1.6183E−08	1.6194E−08	1.61196E-08
2000.00	1.7270E+03	1.7230E+03	1.7245E+03	1.7245E+03	1.7245E+03	1.9187E+03	1.9324E+03	1.9339E+03	1.9340E-03
2500.00	3.1911E+05	3.1853E+05	3.1875E+05	3.1875E+05	3.1875E+05	3.4178E+05	3.4259E+05	3.4280E+05	3.4283E+05
4500.00	3.5631E+09	3.5595E+09	3.5602E+09	3.5602E+09	3.5602E+09	3.6413E+09	3.6396E+09	3.6403E+09	3.6404E+09

TABLE 7: Forward Rate Constants (sec^{-1}) Using MCSCF Level to Scale the PES

T (K)	TST	TST/CAG	CVT	CVT/CAG	ICVT	TST/W	TST/ZCT	CVT/ZCT	ICVT/ZCT
200.00	3.1613E−83	3.2829E−84	3.2489E−84	3.2480E−84	3.4670E−84	2.3691E−82	1.1084E−23	1.0966E−23	1.1705E−23
250.00	5.0671E−64	8.2770E−65	8.1892E−65	8.1873E−65	8.5345E−65	2.6127E−63	1.5115E−23	1.4951E−23	1.5585E−23
298.50	1.6030E−51	3.5149E−52	3.4850E−52	3.4843E−52	3.5821E−52	6.2764E−51	1.9900E−23	1.9726E−23	2.0280E−23
300.00	3.3681E−51	7.4413E−52	7.3788E−52	7.3772E−52	7.5819E−52	1.3089E−50	2.0064E−23	1.9892E−23	2.0443E−23
350.00	5.0312E−42	1.3791E−42	1.3723E−42	1.3720E−42	1.3975E−42	1.5700E−41	2.6255E−23	2.6119E−23	2.6605E−23
400.00	3.9316E−35	1.2670E−35	1.2657E−35	1.2654E−35	1.2815E−35	1.0315E−34	3.4119E−23	3.4078E−23	3.4509E−23
450.00	9.2361E−30	3.3754E−30	3.3858E−30	3.3850E−30	3.4145E−30	2.1084E−29	4.4287E−23	4.4413E−23	4.4800E−23
600.00	5.5464E−19	2.6070E−19	2.6438E−19	2.6428E−19	2.6509E−19	9.5484E−19	5.8476E−19	5.9279E−19	5.9462E−19
800.00	7.5106E−11	4.2636E−11	4.3684E−11	4.3649E−11	4.3705E−11	1.0559E−10	6.3371E−11	6.4877E−11	6.4960E−11
1000.00	6.0791E−06	3.8647E−06	3.9833E−06	3.9778E−06	3.9833E−06	7.6582E−06	4.9261E−06	5.0703E−06	5.0773E−06
2000.00	4.9772E+04	3.9685E+04	3.8383E+04	3.9767E+04	3.8355E+04	5.3004E+04	4.2051E+04	3.1541E+04	4.0642E+04
2500.00	5.0066E+06	4.1769E+06	3.6913E+06	3.0069E+06	3.6906E+06	5.2147E+06	4.3339E+06	3.1199E+06	3.8293E+06
4500.00	1.9026E+10	1.7204E+10	1.2734E+10	1.1318E+10	1.2734E+10	1.9270E+10	1.7400E+10	1.1447E+10	1.2879E+10

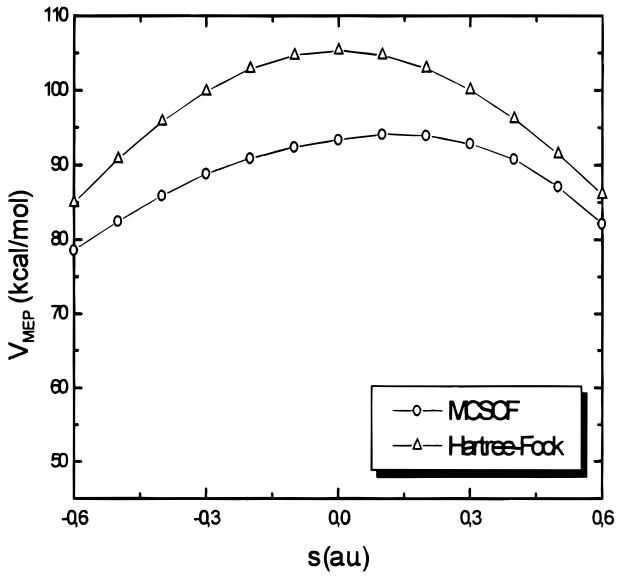

Figure 4. Potential energy curves calculated at Hartree−Fock and MCSCF levels.

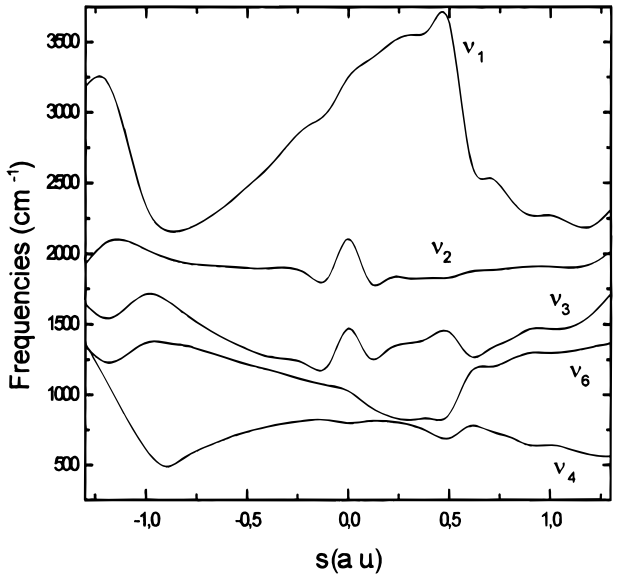

Figure 5. Generalized normal-mode vibrational frequencies as a function of the reaction coodinate, *s*.

published data,[10] and the MC10 value is also compatible with experimental data.[36]

The discrepancy in the calculated vibrational frequencies of the saddle point may cause an error in the description of the potential around the barrier and the forces on the atoms. This error will introduce a further inaccuracy in the variational localization of the transition state and in the calculation of the rate constants.

Reaction Path and Variational Transition State Rate Constants. Figure 3 shows the minimum energy path, V_{MEP}, and the ground-state vibrationally adiabatic potential energy surface, V_a^G, as a function of the coordinate *s*. The ab initio calculated MCSCF points, used as input of the POLYRATE program for the determination of the minimun energy path, are also shown. Figure 4 shows the calculated reaction path at HF and MCSCF levels. The barrier height is lowered drastically (by 16.50 kcal/mol) by introducing correlation effects. Also, the curvature of the reaction path is strongly affected.

The change in the zero-point energy along the reaction path decreases the barrier height by 1.2 kcal/mol at MCSCF level, and thus increases the rate constant by more than a factor of 7 at room temperature and by a factor of about 1.2 at 2500 K.

In Figure 5 the variation of the generalized normal-mode frequencies along the reaction path is shown. In the negative limit of *s* there are six frequencies corresponding to the reactant molecule. In the positive limit there are only two frequencies corresponding to the H_2 + CO products. The harmonic vibrational frequency of the CH−CH stretching, corresponding

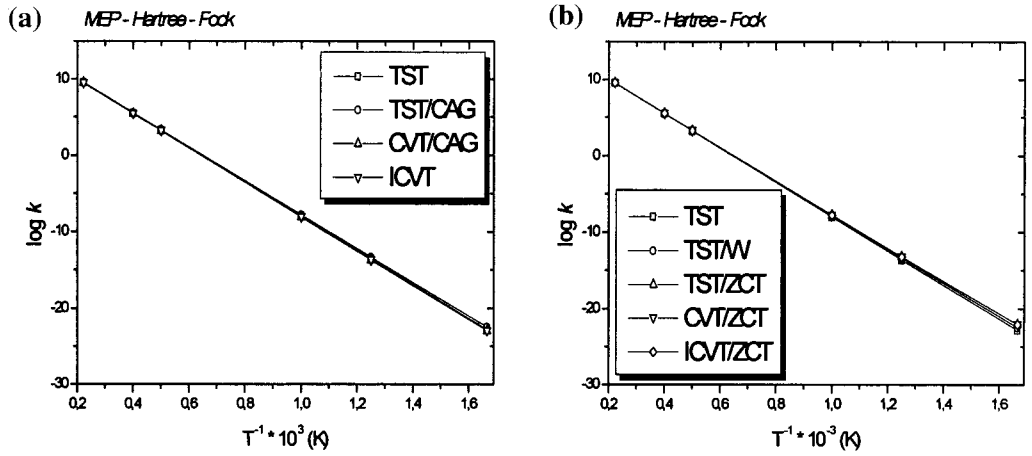

Figure 6. Arrhenius plot using a Hartree−Fock level to scale the MEP, (a) rate constants without tunnel effect and (b) rate constants with two types of approximation to tunnel effect, Wigner(W) and MEPSAG (ZCT).

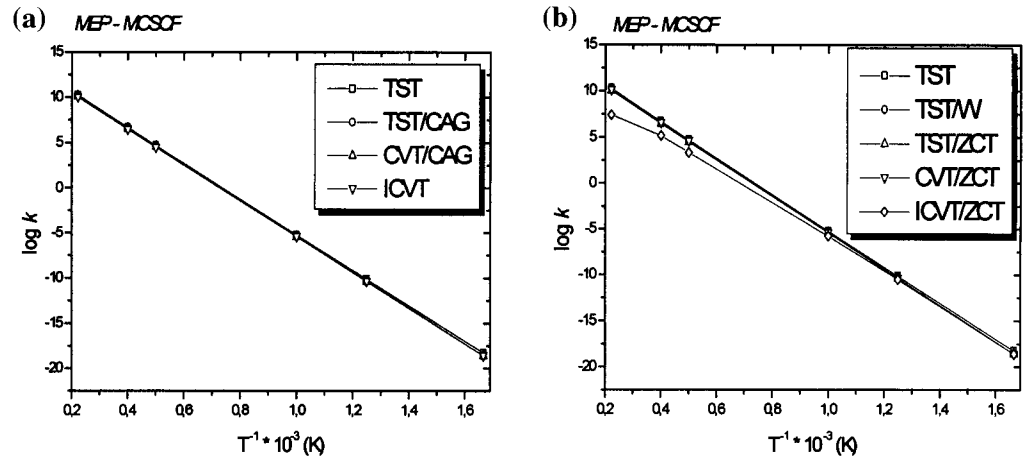

Figure 7. Arrhenius plot using MCSCF level to scale the MEP, (a) rate constants without tunnel effect and (b) rate constants with two types of approximation to tunnel effect, Wigner(W) and MEPSAG (ZCT).

to the normal mode breaking during reaction, drops sharply near the saddle point zone. The MSCF10 imaginary frequency is $1735i$ cm^{-1}.

In Table 5 the bottleneck properties of the reaction, based on the canonical variational transition state approach, are shown. Note that both curves were optimized and the gradients and Hessian matrixes were evaluated. The variational optimization of the generalized transition state dividing surface does not have a large effect on the calculated V_{MEP} at the HF level. As the calculation level is raised, the maximum of s is shifted from $s = 0$. The change in the position of the bottleneck at the MCSCF level between 1000 and 2000 K is very large and seems rather unnusual. In maximizing the free energy of activation, there are two opposing influences: the enthalpy change and the entropy change. Both quantities are maximized at large separations of the fragments in the transition state. Since the entropy term appears as a negative quantity in the free energy change, this term favors a maximum in $\Delta G^{\ddagger}$ at smaller separations of the fragments. The contribution of the $\Delta S^{\ddagger}$ term to the free energy becomes more important as the temperature increases. Hence, the position of the variational transition state should move to smaller separations of the fragments with increasing temperature. This is the general trend of the results in Table 5. Nevertheless, the large effect observed at the MCSCF level may be due to the high sensitivity of the results to the details of the energy surface in the saddle point region, which is largely affected by correlation effects.

In Tables 6 and 7 the calculated rate constants are listed for the temperature range 200−4500 K, using the HF and MCSCF levels to evaluate the MEP. As expected, the conventional TST constants are higher at all temperatures and the zero-point energy contribution increases all rate constants. Using the MCSCF level to scale the PES, the CVT rate constant is 0.22 times the conventional transition state theory at room temperature but the difference is lower at higher temperatures (a factor of 0.59 at 4500 K).

The CVT and ICVT rate constants are quite similar. The difference, mainly at low temperatures, is a consequence of the treatment of the adiabatic potential curves in both methods.

Unpublished results from our laboratory[22] show that a full microcanonical variational treatment of this reaction gives results which are identical to those with the ICVT method.

Tables 6 and 7 and Figures 6 and 7 also show large tunneling effects. The large imaginary barrier frequency and the calculated geometric parameters for the saddle point suggest that this reaction primarily involves the motion of hydrogen atoms and tunneling contribution may be significant. Finally, Figure 8 shows the generalized standard-state free energy calculated as a function of s for several temperatures. These curves follow the general trend shown by the potential energy curves (Figure 5). As previously stated, within the variational approach, the localization of the dividing surface is done using the maximum free energy criterium.

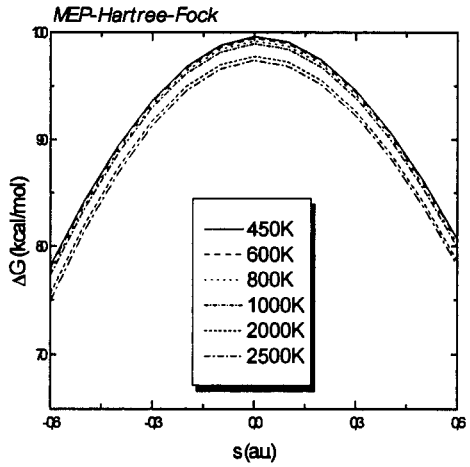

Figure 8. Generalized standard-state free energy of activation (kcal/mol) as a function of the reaction coordinate for six values of temperatures.

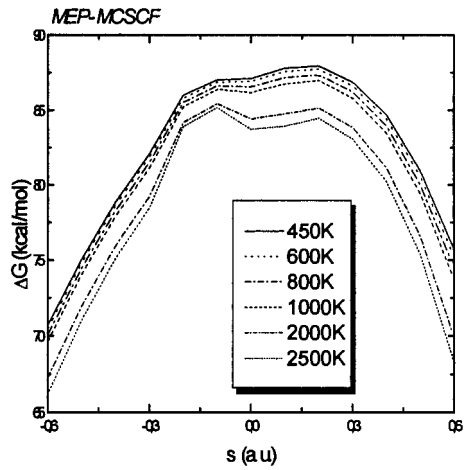

Figure 9. Generalized standard-state free energy of activation (kcal/mol) as a function of the reaction coordinate for six values of temperatures.

One of the main difficulties in the interpretation of the calculated kinetic results is the lack of experimental canonical rate constant values since at the temperatures of interest the reaction does not occur thermally. Also, a fundamental requirement for the application of canonical TST is that the reactant molecules are distributed over energy states according to the Maxwell−Boltzmann laws. This is true only for thermal systems in the high-pressure limit. To our knowledge, a canonical TST calculation has not been carried out before.

In a second paper,[22] both the microcanonical variational transition state theory and the RRKM with tunneling corrections approaches will be presented for this system. The unimolecular high-pressure constants calculated on the basis of the RRKM results and the microcanonical variational transition state theory are in agreement with the results of this paper. The excitation energy from the ground vibrational state of the S_0 state of formaldehyde to the ground vibrational state of the S_1 is 80.6 kcal/mol.[1−2] The microcanonical rate constant[22] calculated for the total energy resulting from this excitation is about 1×10^9 s^{-1}. Assuming that the excited electronic state S_1 undergoes a radiationless transition back to S_0 states a vibrational temperature of 3900−4000 K may be estimated. As shown in Figure 6, the ICVT rate constants for this temperature range are 1×10^9 to 1×10^{10} s^{-1}.

Certainly, this is a very crude approximation and the microcanonical rate constants are not directly comparable, but these considerations may be interpreted as an estimation of the vibrational temperature of the experimental system.

Conclusions

To calculate the rate constants for formaldehyde decomposition using the generalized transition state theory, the stationary points and the reaction path were computed at high levels of theory. The MCSCF barrier is 83.2 kcal/mol, in good agreement with previously calculated results.[10] Also, the agreement with the experimental S_1 origin of 80.6 kcal/mol is fairly acceptable. As the level is raised, the barrier height is lowered and the maximum of *s* shifts toward the reactants. This is probably not a variational effect but is due to the sensitivity of the saddle point region to correlation effects.

Tunneling effects and zero-point vibrational energy along the reaction path are of primary importance for this reaction.The direct dynamics approach seems suitable for treating this reaction. Unfortunately, there are no experimental or calculated canonical rate data for this system to compare with the present results.

Acknowledgment. The authors acknowledge partial financial support by FAPERJ, CNPq, and FINEP and the computational facilities at NCE/UFRJ. They also thank Professor Marco Antonio Chaer Nascimento for many valuable discussions and suggestions and for his interest in this work.

References and Notes

(1) Young, E. S.; Moore, C. B. *J. Chem. Phys*. **1973**, *58*, 3988.
(2) Houston, P. L.; Moore, C. B. *J. Chem. Phys*. **1976**, *65*, 757.
(3) Moore, C. B.; Weisshaar, J. C. *Annu. Rev. Phys. Chem*. **1983**, *34*, 525.
(4) Bamford, D. J.; Filseth, S. V.; Foltz, M. F.; Hepburn, J. W.; Moore, C. B. *J. Chem. Phys*. **1985**, *82*, 3032.
(5) Debarre, D.; Lefebre, M.; Péalat, M.; Taran, J. P. E.; Bamford, D. J.; Moore, C. B. *J. Chem. Phys*. **1985**, *83*, 4476.
(6) Butenhoff, T. J.; Carleton, K. L.; Moore, C. B. *J. Chem. Phys*. **1990**, *92*, 377.
(7) Terentis, A. C.; Kable, S. H. *Chem. Phys. Lett*. **1996**, *258*, 626.
(8) Goddard, J. D.; Schaefer, H. F., III *J. Chem. Phys*. **1979**, *70*, 5117; see also references cited therein.
(9) Goddard, J. D.; Yamaguchi, Y.; Schaefer, H. F., III *J. Chem. Phys*. **1981**, *75*, 3459.
(10) Dupuis, M.; Lester, W. A., Jr.; Lengsfield, B. H., III; Lui, B. *J. Chem. Phys*. **1983**, *79*, 6167.
(11) Frisch, M. J.; Binkley, J. S.; Schaefer, H. F., III *J. Chem. Phys*. **1984**, *81*, 1882.
(12) Scuseria, G. E.; Schaefer, H. F., III *J. Chem. Phys*. **1989**, *90*, 3629.
(13) Green, W. H., Jr.; Willetts, A.; Jayatilaka, D.; Handy, N. C. *Chem. Phys. Lett*. **1990**, *169*, 127.
(14) Frisch, M. J.; Krishnan, K.; Pople J. A. *J. Phys. Chem*. **1981**, *85*, 1467.
(15) Chang, Y. T.; Minichino, C.; Miller, W. H. *J. Chem. Phys*. **1992**, *96*, 4341.
(16) Peslherbe, G. H.; Hase, W. L. *J. Chem. Phys*. **1996**, *104*, 7882.
(17) Miller, W. H. *J. Am. Chem. Soc*. **1979**, *101*, 6810.
(18) Troe, J. *J. Phys. Chem*. **1984**, *88*, 4375.
(19) Truhlar, D. G.; Isaacson, A. D.; Garrett, B. C. Generalized Transition State Theory. In *The Theory of Chemical Reaction Dynamics*; Baer, M., Ed.; CRC Press: Boca Raton, FL, 1985; Vol. 4, pp 65−137.
(20) Baldridge, K. M.; Gordon, M. S.; Steckler, R.; Truhlar, D. G. *J. Phys. Chem*. **1989**, *93*, 5107.
(21) Liu, Y.-P.; Lynch, G. C.; Truong, T. N.; Lu, D.-h.; Truhlar, D. G.; Garrett, B. C. *J. Am. Chem. Soc*. **1993**, *115*, 2408.
(22) Martins, L. M. M. de A.; Arbilla, G.; Silva, E. C. da. To be published.
(23) (a) Huzinaga, S. *J. Chem. Phys*. **1965**, *42*, 1293. (b) Dunning, T. H. *J. Chem Phys*. **1970**, *53*, 2823.
(24) Dupuis, M.; Wendolowiski, J. J.; Spangler, D. *Natl. Resour. Comput. Chem. Software*, Catal. 1, Prog. No. OG01, 1980.
(25) (a) Stecker, R.; Hu, W. P.; Liu, Y. P.; Lynch, G. C.; Garrett, B. C.; Isaacson, A. D.; Lu, D. H.; Melissas, V. S.; Truong, T. N.; Rai, S. N.; Hancock, G. C.; Lauderdale, J. G.; Joseph, T.; Truhlar, D. G. *POLYRATE, Version 6.2*, University of Minneapolis, 1994. (b) Chuang, Y.-Y.; Coitiño,

E. L.; Hu, W.-P.; Liu, Y.-P.; Lynch, G. C.; Nguyen, K. A.; Jackels, C. F.; Gu, M. Z.; Rossi, I.; Fast, P.; Clayton, S.; Melissas, V. S.; Garrett, B. C.; Isaacson, A. D.; Truhlar, D. G. *POLYRATE, Version 7.0*, University of Minneapolis, 1996.

(26) Gilbert, R. G.; Smith, S. C. *Theory of Unimolecular and Recombination Reactions*; Blackwell Scientific Publications: Oxford, 1990.

(27) Baker, J. *J. Comput. Chem*. **1986**, *7*, 385.

(28) Cerjan, C. J.; Miller, W. H. *J. Chem. Phys*. **1981**, *75*, 2800.

(29) Miller, W. H.; Handy, N. C.; Adams, J. E. *J. Chem. Phys*. **1980**, *72*, 99.

(30) Truhlar, D. G.; Kuppermann, A. *J. Chem. Phys*. **1970**, *52*, 3842.

(31) Truhlar, D. G.; Kuppermann, A. *J. Am. Chem. Soc*. **1971**, *93*, 1840.

(32) Garrett, B. C.; Truhlar, D. G.; Grev, R. S.; Magnuson, A. W. *J. Phys. Chem*. **1980**, *84*, 1730.

(33) Lu, D. H.; Truong, T. N.; Melissas, V. S.; Lynch, G. C.; Liu, Y. P.; Garrett, B. C.; Steckler, R.; Isaacson, A. D.; Rai, S. N.; Hancock, G.; Lauderdale, J. G.; Joseph, T.; Truhlar, D. G. *Computer Phys. Comm.***1992**, *71*, 235.

(34) Skodje, R. T.; Truhlar, D. G.; Garrett, B. C. *J. Phys. Chem.* **1981**, *85*, 3019.

(35) Liu, Y. P.; Lynch, G. C.; Truong, T. N.; Lu, D. H.; Truhlar, D. G. *J. Am. Chem. Soc*. **1993**, *115*, 2408.

(36) Yamada, K.; Nakagawa, T.; Kuchitsu, K.; Morino Y. *J. Mol. Spectrosc*. **1971**, *38*, 70.

(37) Miller, W. H. *J. Am. Chem. Soc.* **1979**, *101*, 6810.

(38) Miller, W. H. *Chem. Rev.* **1987**, *87*, 19.

(39) Frost, W. *J. Phys. Chem.* **1983**, *87*, 4489.